Table S1. Iron fractions in Bdg and Fp. The values are calculated based on the previously determined iron partition coefficients for a pyrolitic mantle (Irifune et al., 2010). Previous studies (Wang et al., 2015; Wu, 2016; Zhang et al., 2016) suggested that the lower mantle may be represented by a pyrolitic composition (78 vol% Bdg+15 vol% Fp) with ~ 8 wt% FeO (McDonough and Sun, 1995).

Pressure (GPa)	K_D	n_{Bdg}	n_{Fp}
23.1	0.57	0.59	0.41
24.9	0.64	0.61	0.39
26.6	0.71	0.64	0.36
27.4	0.75	0.65	0.35
29.5	0.8	0.66	0.34
32.9	0.84	0.67	0.33
35.9	0.85	0.67	0.33
38.8	0.84	0.67	0.33
40.2	0.82	0.67	0.33
42.0	0.76	0.65	0.35
43.9	0.63	0.61	0.39
45.6	0.58	0.59	0.41
48.0	0.52	0.57	0.43
50.7	0.49	0.56	0.44
55.6	0.46	0.54	0.46
60.0	0.45	0.54	0.46
68.5	0.42	0.52	0.48
74.3	0.41	0.52	0.48
80.7	0.4	0.51	0.49
89.6	0.39	0.51	0.49
95.9	0.39	0.51	0.49
104.6	0.39	0.51	0.49
122.5	0.39	0.51	0.49

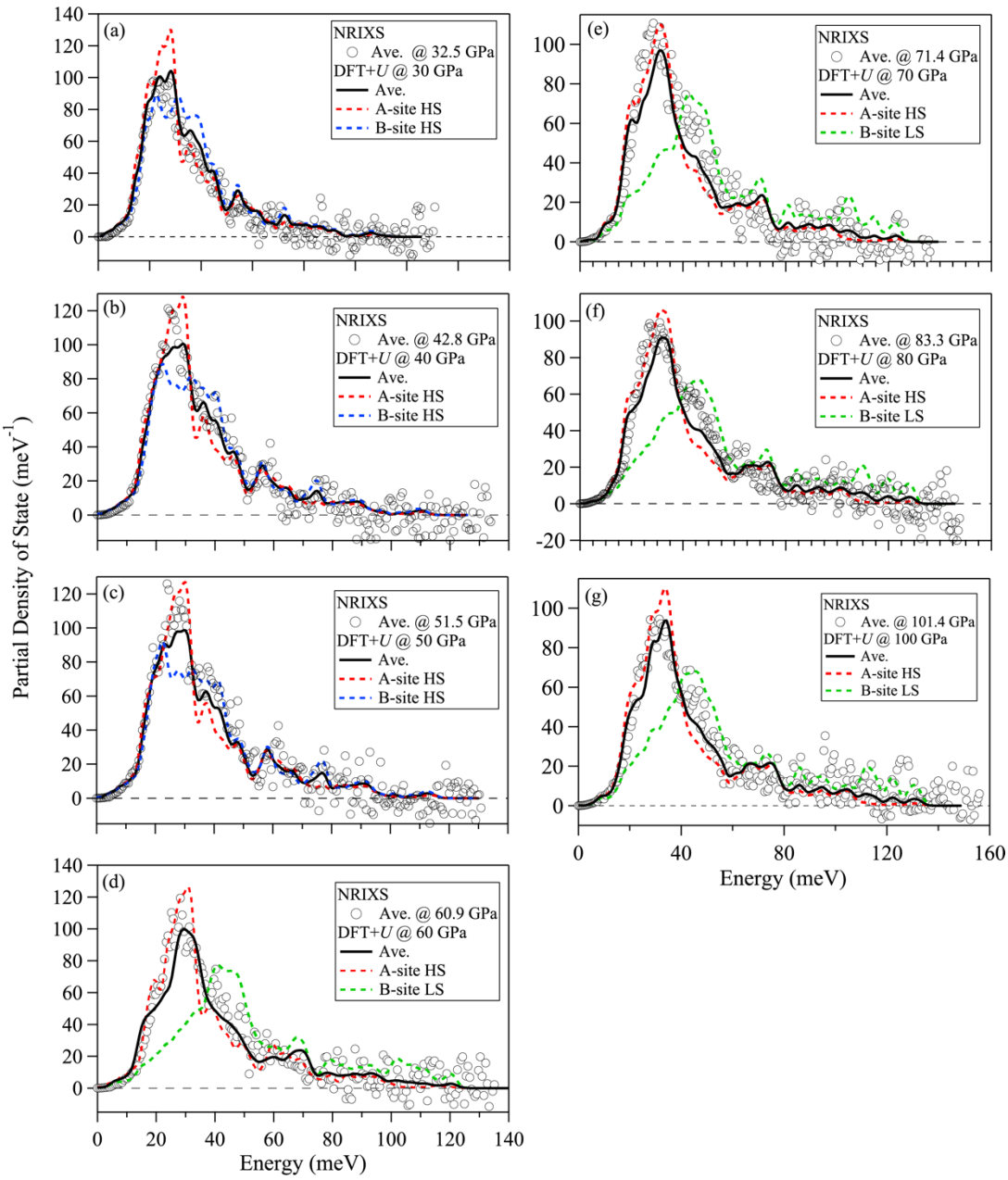

Figure S1. The comparison of 300-K partial phonon density of states (PDOS) of Fe^{3+} in $(Mg_{0.5}Fe^{3+}_{0.5})(Si_{0.5}Fe^{3+}_{0.5})O_3$ bridgmanite derived from both NRIXS measurements and DFT + *U* calculations. The open circles are the averaged PDOS of A-site Fe^{3+} and B-site Fe^{3+} measured by NRIXS. The red dotted, blue dashed and green dashed curves are the PDOS of A-site HS Fe^{3+}, B-site HS Fe^{3+} and B-site LS Fe^{3+} calculated by DFT + *U* method. The black curves are the weighted average of the PDOS of the A-site and B-site Fe^{3+} from DFT + *U* calculations. The weights are equal for A-site HS and B-site HS Fe^{3+} configuration while the proportions are 70% and 30% for A-site HS and B-site LS Fe^{3+} configuration.

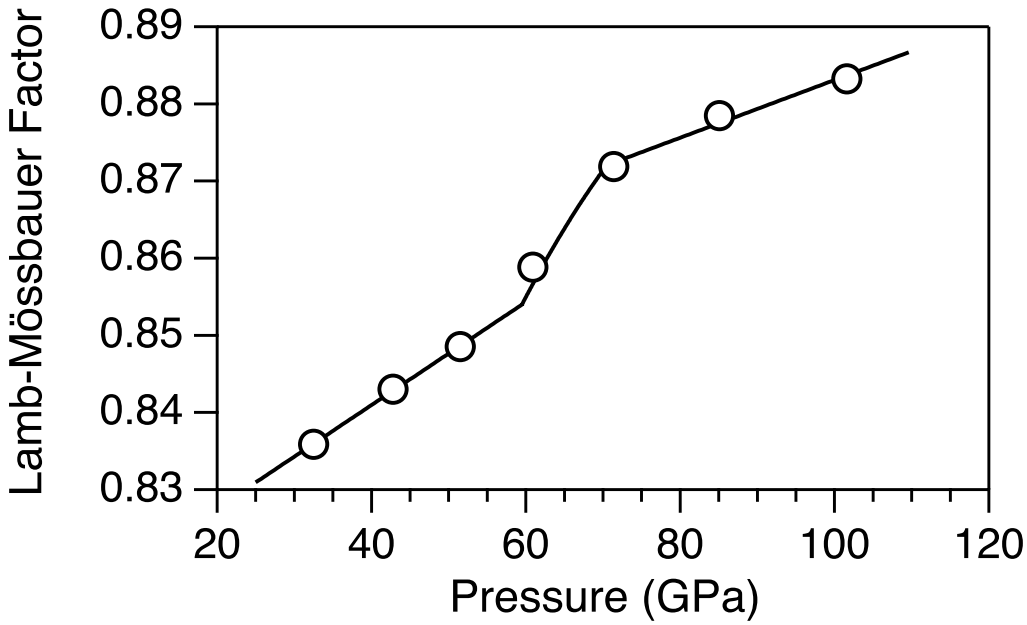

Figure S2. The pressure dependence of the Lamb-Mössbauer factor (*f*) of $(Mg_{0.5}Fe^{3+}_{0.5})(Si_{0.5}Fe^{3+}_{0.5})O_3$ bridgmanite at 300 K. Across the spin transition of B-site Fe^{3+}, the Lamb-Mössbauer factor increases significantly, reflecting the decrease of inelastic component in the NRIXS spectra. The black curve is modeled averaged *f* by incorporating the low spin fraction (n_{LS}) across the spin transition pressures ($f = f_{HS} \times n_{HS} + f_{LS} \times n_{LS}$).

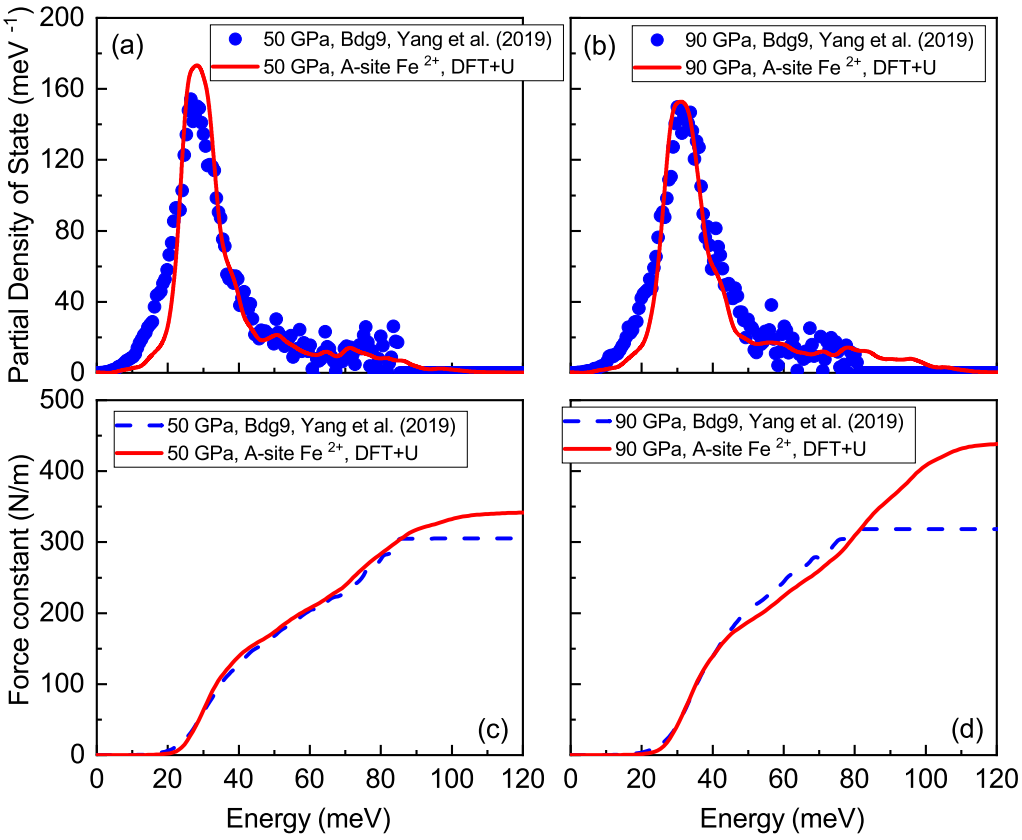

Figure S3. (a) (b) calculated PDOS of A-site Fe^{2+} in $(Mg_{0.75}Fe^{2+}_{0.25})SiO_3$ and $(Mg_{0.5}Fe^{2+}_{0.5})SiO_3$ bridgmanite compared with experimental PDOS of $Mg_{0.92}Fe^{2+}_{0.07}Fe^{3+}_{0.02}Si_{0.99}O_3$ bridgmanite (Bdg9, Fe dominantly occurs as A-site Fe^{2+}) from Yang et al. (2019). $(Mg_{0.75}Fe^{2+}_{0.25})SiO_3$ and $(Mg_{0.5}Fe^{2+}_{0.5})SiO_3$ bridgmanite have almost the same PDOS. The predicted PDOS from DFT+*U* calculations agree well with experimental measurements. **(c) (d)** the evolution of <*F*> with the upper limit of energy (*x*) for the integration $< F >= \frac{M}{\hbar^2}\int_0^x E^2\, g(E)dE$. The integral values of <*F*> from calculated PDOS agree well with those from experimental PDOS until energy for the integration reaches a threshold, above which the predicted <*F*> still increases with *x* but the experimental one maintains a constant value. The final <*F*> calculated from theoretical PDOS at 90 GPa is significantly larger than the experimental one by ~130 N/m due to the low signal noise ratio at the high-energy part of experimental PDOS.

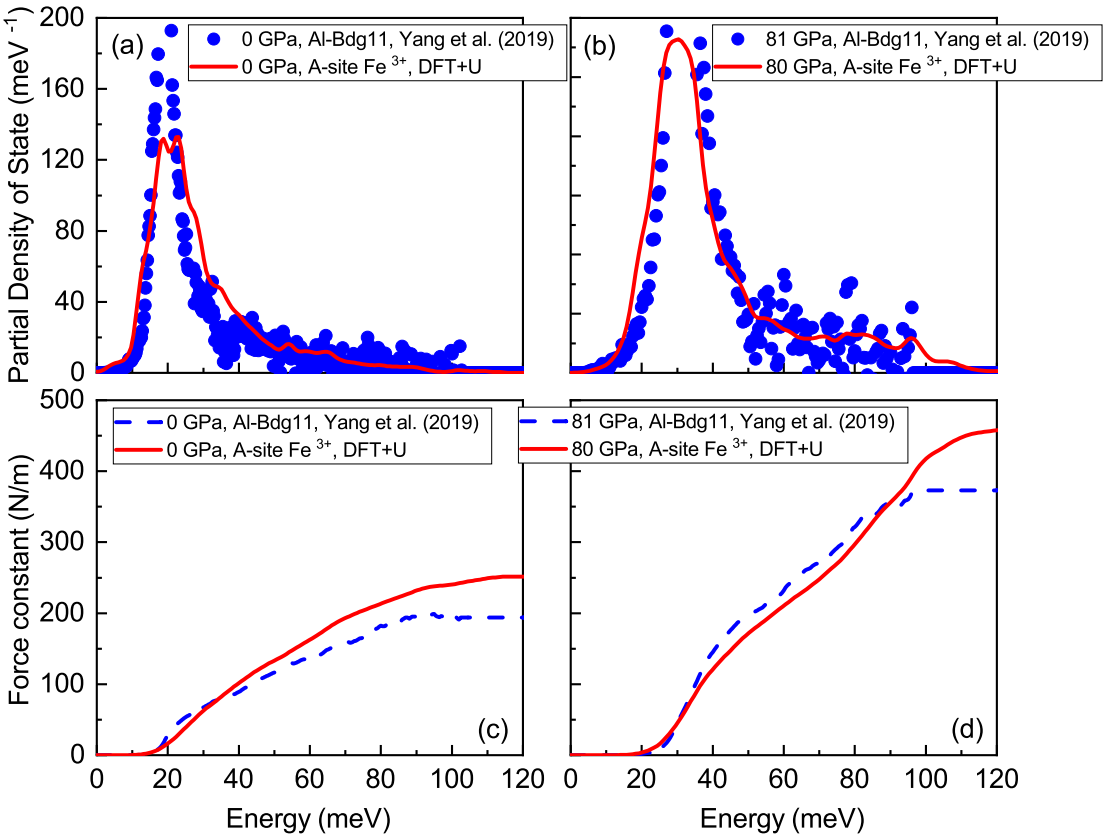

Figure S4. (a) (b) calculated PDOS of A-site Fe^{3+} in $(Mg_{0.75}Fe^{3+}_{0.25})(Si_{0.75}Al_{0.25})O_3$ and $(Mg_{0.9375}Fe^{3+}_{0.0625})(Si_{0.9375}Al_{0.0625})O_3$ bridgmanite compared with experimental PDOS of $Mg_{0.89}Fe^{2+}_{0.024}Fe^{3+}_{0.096}Al_{0.11}Si_{0.89}O_3$ bridgmanite (Al-Bdg11, Fe dominantly occurs as A-site Fe^{3+}) from Yang et al. (2019). PDOS of Fe in $(Mg_{0.75}Fe^{3+}_{0.25})(Si_{0.75}Al_{0.25})O_3$ is almost the same as that in $(Mg_{0.9375}Fe^{3+}_{0.0625})(Si_{0.9375}Al_{0.0625})O_3$. **(c) (d)** the evolution of $<F>$ with the upper limit of energy (x) for the integration $< F >= \frac{M}{\hbar^2}\int_0^x E^2\, g(E)dE$. Although the predicted PDOS from DFT+U calculations agree well with experimental measurements, the final $<F>$ calculated from theoretical PDOS are significantly larger than those calculated from experimental PDOS mainly due to the low signal noise ratio at the high-energy part of experimental PDOS. The $<F>$ differences are ~ 50 N/m at 0 GPa and ~ 100 N/m at 80 GPa.

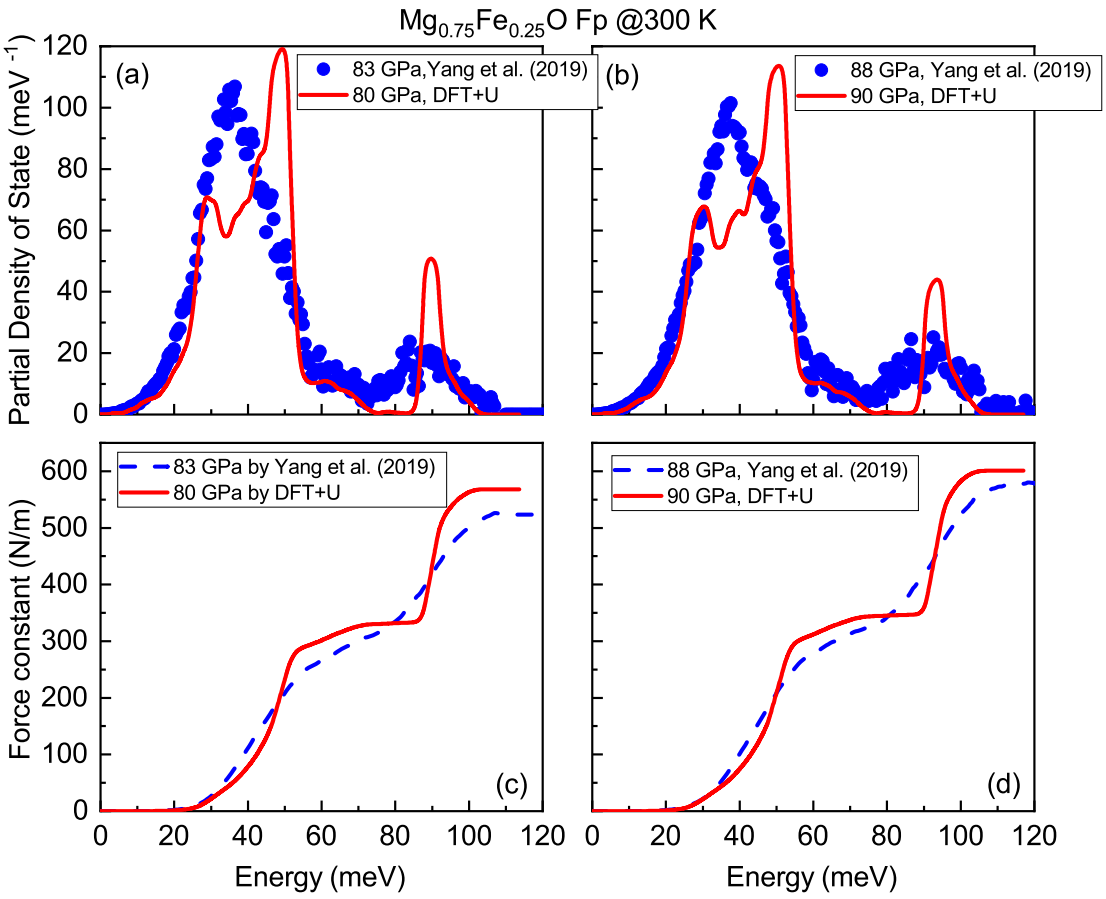

Figure S5. (a) (b) predicted PDOS of low-spin Fe^{2+} in $(Mg_{0.75}Fe^{2+}_{0.25})O$ from DFT+U calculations compared with experimental PDOS from Yang et al. (2019). **(c) (d)** the evolution of <*F*> with the upper limit of energy (*x*) for the integration $< F >= \frac{M}{\hbar^2}\int_0^x E^2\, g(E)dE$. Both of calculated PDOS and <*F*> agree well with experimental results.

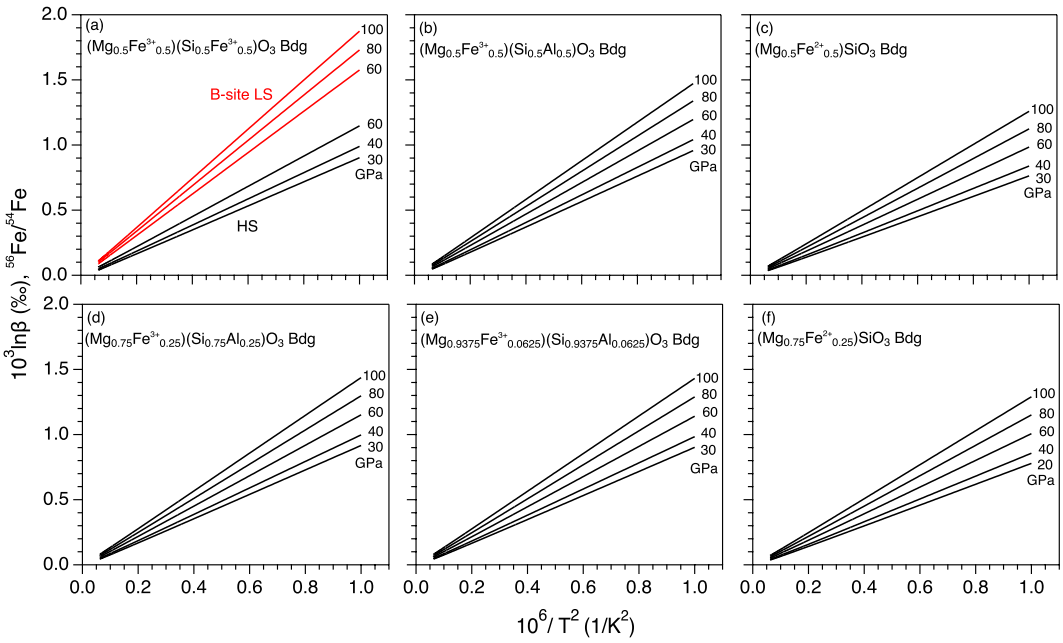

Figure S6. The temperature-dependence of the $^{56}Fe/^{54}Fe$ β-factors of various bridgmanite compositions. In (a), the black curves are for high-spin $(Mg_{0.5}Fe^{3+}_{0.5})(Si_{0.5}Fe^{3+}_{0.5})O_3$ Bdg at and below 60 GPa; the red curves are for B-site low-spin $(Mg_{0.5}Fe^{3+}_{0.5})(Si_{0.5}Fe^{3+}_{0.5})O_3$ Bdg at and above 60 GPa.

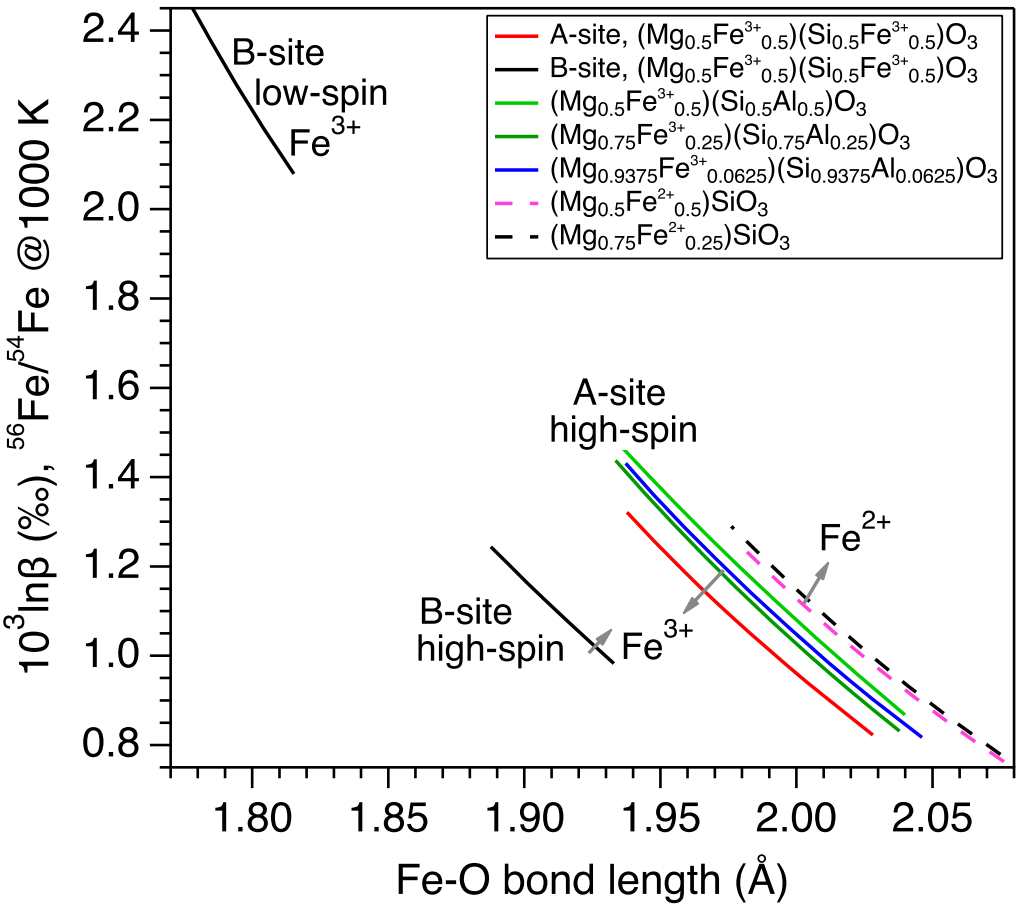

Figure S7. The relationship between the 1000-K $^{56}Fe/^{54}Fe$ β-factors and the Fe-O bond length of bridgmanite with different compositions at 30-100 GPa by DFT+U calculations.

References

Irifune, T., Shinmei, T., McCammon, C.A., Miyajima, N., Rubie, D.C., Frost, D.J., 2010. Iron Partitioning and Density Changes of Pyrolite in Earth's Lower Mantle. Science (80-.). 327, 193–195. doi:10.1126/science.1181443

McDonough, W.F., Sun, S. -s., 1995. The composition of the Earth. Chem. Geol. 120, 223–253. doi:10.1016/0009-2541(94)00140-4

Wang, X., Tsuchiya, T., Hase, A., 2015. Computational support for a pyrolitic lower mantle containing ferric iron. Nat. Geosci. 8, 556–559. doi:10.1038/ngeo2458

Wu, Z., 2016. Velocity structure and composition of the lower mantle with spin crossover in ferropericlase. J. Geophys. Res. Solid Earth 121, 2304–2314. doi:10.1002/2015JB012667

Zhang, S., Cottaar, S., Liu, T., Stackhouse, S., Militzer, B., 2016. High-pressure, temperature elasticity of Fe- and Al-bearing MgSiO3: Implications for the Earth's lower mantle. Earth Planet. Sci. Lett. 434, 264–273. doi:10.1016/j.epsl.2015.11.030